Application of van der Waals functionals to the calculation of dissociative adsorption of N_2 on W(110) for static and dynamic systems

Davide Migliorini,[1, a)] Francesco Nattino,[1] and Geert-Jan Kroes[1]

[1] *Leiden Institute of Chemistry, Leiden University, Gorlaeus Laboratories, P.O. Box 9502 2300 RA Leiden, The Netherlands*

(Dated: September 12, 2016)

[a)] Email: d.migliorini@lic.leidenuniv.nl

ABSTRACT

The fundamental understanding of molecule-surface reactions is of great importance to heterogeneous catalysis, motivating many theoretical and experimental studies. Even though much attention has been dedicated to the dissociative chemisorption of N_2 on tungsten surfaces, none of the existing theoretical models has been able to quantitatively reproduce experimental reaction probabilities for the sticking of N_2 to W(110). In this work, the dissociative chemisorption of N_2 on W(110) has been studied with both static electronic structure and *ab initio* molecular dynamics (AIMD) calculations including the surface temperature effects through surface atom motion. Calculations have been performed using density functional theory (DFT), testing functionals that account for the long range van der Waals (vdW) interactions, which were previously only considered in dynamical calculations within the static surface approximation. The vdW-DF2 functional improves the description of the potential energy surface (PES) for N_2 on W(110), returning less deep molecular adsorption wells and a better ratio between the barriers for the indirect dissociation and the desorption, as suggested by previous theoretical work and experimental evidence. Using the vdW-DF2 functional less trapping-mediated dissociation is obtained compared to results obtained with standard semi-local functionals such as PBE and RPBE, improving agreement with experimental data at $E_i = 0.9$ eV. However, at $E_i = 2.287$ and off-normal incidence, the vdW-DF2 AIMD underestimates the experimental reaction probabilities, showing that also with the vdW-DF2 functional the N_2 on W(110) interaction is not yet described with quantitative accuracy.

I. INTRODUCTION

Heterogeneous catalysis plays an important role in many industrial processes[1,2]. Many experimental and theoretical studies have been performed in order to improve the fundamental understanding of molecular reactions on metal surfaces, since this knowledge can help with the development of more efficient catalysts. Among the industrial processes that make use of heterogeneous catalysis, one of the most important is the Haber-Bosch process that is used to produce ammonia from the reaction of N_2 and H_2 on an iron based catalyst[3]. The dissociation of N_2, catalyzed by the metal surface, is believed to be the rate-determining

step of the whole process[3] motivating the interest for this reaction step. The dissociation probability of N_2 on an iron single crystal surface shows a clear dependence on the crystallographic face of the metal on which the reaction occurs[4]. Similarly, tungsten surfaces show an high crystallographic anisotropy of the nitrogen dissociation probability (S_0): it is known, from molecular beam experiments, that for low collision energies (E_i) the W(100) surface is roughly two orders of magnitude more reactive than the W(110) surface[5]. The observed non-zero reaction probability of N_2 on W(100) for vanishing E_i suggested that, on this surface, non-activated paths for the dissociation exist[6,7]. For N_2 on W(110)[7,8] the measured reaction probability is almost zero (i.e., $\approx 10^{-3}$) at low E_i and increases with increasing collision energy, which suggested an activated mechanism for the dissociative chemisorption. The similarity of N_2 on W and the catalytically more relevant Fe surface (the crystallographic anisotropy of the N_2 dissociation) has prompted many studies on N_2 dissociation on W surfaces. Even though much attention has been dedicated to the theoretical study of the dissociative chemisorption of N_2 on tungsten surfaces, none of the existing models has been able to quantitatively reproduce experimental reaction probabilities for the sticking of N_2 to W(110).

In a previous work Alducin *et al.*[9,10], even tough that the S_0 curve shape suggests an activated reaction path, achieved a qualitative description of the dissociation probability of N_2 on W(110) through molecular dynamics calculations performed on a potential energy surface (PES) that also included non-activated paths for dissociation. Alducin *et al.*[9,10] and Bocan *et al.*[11] computed the reaction probability on two PESs calculated with density functional theory (DFT) at the generalized gradient approximation (GGA) level, using the PW91[12,13] functional and the RPBE functional[14], respectively. These dynamical calculations used the ideal static surface approximation. Different functionals gave better agreement with experiments in different experimental conditions: using the more repulsive RPBE functional good agreement with experimental results was found for normal incidence ($\Theta_i = 0°$), but the reaction probability at $\Theta_i = 60°$ was underestimated. The PW91 functional returned good agreement with experimental data at $\Theta_i = 60°$ but it failed at describing experiments at normal incidence, with the reaction probability being too high at low E_i. This behavior can be due on the one hand to the fact that the more repulsive RPBE functional returns good barrier heights for the indirect dissociation achieving a better agreement with experiments for normal incidence where this mechanism dominates but failing to reproduce experimental

data off-normal incidence. On the other hand the less repulsive PBE functional returns lower barrier for the direct dissociation that means a better agreement with experiments off-normal incidence but the molecular adsorption states are too strongly bond to the surface resulting in an high indirect reaction at normal incidence overestimating the experimental data. The results showed that the dissociative chemisorption of N_2 on W(110) is very sensitive to the "shape" of the PES, which determines to what extent the minimum energy paths for dissociation are accessible to the impinging molecules. The results also showed that, in the framework of DFT, the theoretical S_0 strongly depends on the exchange-correlation functional (XC) chosen for the electronic structure calculations and how difficult is to deal with and properly describe reactions that depends on more than barrier like the dissociative chemisorption of N_2 on W(100) .

The importance of modeling surface atom motion for this reaction was demonstrated[15] with *ab initio* molecular dynamics (AIMD) calculations, testing both the RPBE and the PBE[16] functionals. Using the PBE functional (which is similar[16] to the PW91 functional[12,13] used in Ref.[10]) the reaction probability at normal incidence and $E_i = 0.9$ eV is even larger than for the static surface calculations using PW91. This is because the large amount of energy transferred from the impinging molecules to the surface phonons stabilizes molecules trapped on the surface, thereby enhancing the contribution of a trapping-mediated dissociation mechanism to the reactivity. The RPBE functional gives a better agreement with the experiment for $E_i = 0.9$ eV at normal incidence. The AIMD reaction probabilities computed with PBE and RPBE showed little dependence on E_i, in disagreement with experiments. The authors suggested that the reason of this discrepancy is that both the PBE and the RPBE functionals return too deep molecular adsorption wells. The authors also showed that surface atom motion and energy exchange with the surface can not be neglected in modeling the dissociation of N_2 on W(110).

In order to further improve the theoretical description of N_2 on W(110) Martin-Gondre et al. tested different functionals that account for the vdW interaction[17]. The authors performed a static study of some vdW functionals and computed reaction probability for a few energies with AIMD in the frozen surface approximation (AIMD-FS). Some of the functionals studied improve the static properties of the PES, giving less deep molecular adsorption wells and returning barriers for the desorption and for the dissociation from the molecular adsorption states closer to each other than found with semi-local functionals, in better

agreement with experimental evidence[18]. However, the dissociation probabilities calculated with AIMD-FS using the vdW functionals considered did not show better agreement with experiments than the previously used semi-local functionals (i.e., PBE and RPBE).

Two of the most promising functionals that were identified through static calculation are the vdW-DF[19] and the vdW-DF2[20] functionals. The latter, which has not been tested yet in dynamic simulations, is particularly interesting regarding the depth of the molecular adsorption wells and the balance between desorption and dissociation of N_2 from these wells. On the other hand the vdW-DF2 functional shows high barriers for the direct dissociation, which are located far from the surface, just like the RPBE functional. Therefore the vdW-DF2 functional might provide a good description of the reaction at normal incidence. Moreover the attractive long-range van der Waals interactions might improve the agreement with experiments at off-normal incidence.

Here we have extended the static analysis of the N_2+W(110) PES also considering other molecular adsorption minima[15] than considered in Ref.[17] and testing both the vdW-DF and the vdW-DF2 functionals. We have also performed AIMD calculations for N_2 impinging on the W(110) surface using the vdW-DF2 functional, simultaneously accounting for both the effect of the long range vdW interactions and the effect of surface atom motion on the dissociation probability. Our work is part of a larger effort to construct semi-empirical density functionals for a range of molecule-metal surface systems, with the ultimate aim of constructing a database of chemically accurate reaction barriers for these systems[21].

We found that, even though the vdW-DF2 functional seems to return a PES that is in better agreement with the experimental evidence[18], AIMD calculations using this functional still fail at quantitatively reproducing the molecular beam experiments. The vdW-DF2 functional generally gives better agreement with experimental results for $E_i = 0.9$ eV, but the agreement is less good for higher E_i values, especially at off-normal incidence, suggesting that this functional might still be too repulsive far from the surface to reproduce accurately the barriers for the direct dissociation. As for the previously tested semi-local functionals[15], the vdW-DF2 functional returns almost flat reaction probability curves, showing little dependence on incidence energy.

This paper is organized as follows. Section II describes the methodology. In Section III the results are reported and discussed in two subsections: Section III A describes the static study of the PES, including the molecular adsorption states and the barriers involved in

the reaction process, and Section III B reports and analyzes the AIMD results. Section IV summarizes the results and the main conclusions of this work.

II. METHOD

All the electronic structure calculations have been performed using the Vienna Ab Initio Simulation Package (VASP) DFT code[22–25]. The basis set employed includes plane waves with a kinetic energy lower than 450 eV. Tungsten is a body centered cubic (bcc) metal and the W(110) surface has been simulated by a 5 layer slab using a (2x2) surface unit cell. The slab is separated from its periodic image by a 14 Å vacuum. The first Brillouin zone has been sampled by a Γ-centered 8x8x1 k-point grid. To facilitate the electronic convergence a Fermi smearing with a width parameter of 0.1 eV has been used. The core electrons have been modeled using the projected augmented wave (PAW) method[25,26]. For tungsten the six valence electrons have been modeled as active while the other electrons have been frozen in the core. We have also tested the PAW implementation which models 6 additional semi-core p electrons as active electrons, but the equilibrium lattice constant for bulk W and the relaxed interlayer distances in the W(110) surface did not considerably change from the 6-active-electrons-PAW results. Furthermore, molecular adsorption energies calculated with vdW-DF2 using the two different PAW implementations differ by less than 26 meV in agreement with tests performed for semi-local functionals[15]. The dimension of the supercell has been also carefully tested on the molecular adsorption energy and on one of the barriers involved in the dissociation. Increasing the supercell from the 2x2, which we have used, to the 3x3 changes the barrier height for the dissociation from the hollow-parallel molecular adsorption site by only 25 meV. In our study we have simulated molecules impinging on the surface at normal and off-normal incidence. In the latter simulations is possible that the molecule bounces on the surface and then bounces again in the next unit cell on a surface that is periodically perturbed cell. However has been shown that the distortion of the surface does not significantly affect the reactivity of N_2 on W(110). AIMD simulations on a frozen surface but with the atoms displaced like in the moving surface calculations[15] have given the same results (within error bars) of dynamics on the ideal frozen surface (computed by Alducin et al.[10]) suggesting the small effect on reactivity of the surface distortion and justifying the use of the smaller 2x2 supercell.

The calculations have been performed using the vdW-DF2 functional developed by Lee et al.[20] as efficiently implemented in the VASP code[27,28]. The vdW-DF functional[19] has been tested too but only in the static calculations.

The equilibrium tungsten lattice constant has been calculated as 3.183 and 3.238 Å with the vdW-DF and vdW-DF2 functionals, respectively, as compared with the experimental low-temperature value of 3.163 Å[29]. Molecular adsorption energies (E_{ads}) and dissociation energies (E_{diss}) have been computed as:

$$E_{ads} = \epsilon_{ads} - \epsilon_{asym}, \tag{1}$$

$$E_{diss} = \epsilon_{diss} - \epsilon_{asym}, \tag{2}$$

where ϵ_{asym} is the absolute energy of the molecule in its equilibrium geometry placed halfway between two periodic replicas of the slab, ϵ_{ads} is the absolute energy of the molecule in the adsorption configuration and ϵ_{diss} is the absolute energy of the two N atoms in the dissociation configuration. We verified that, in the asymptotic configuration, ϵ_{asym} does not depend on the orientation of the molecule and that, even by doubling the vacuum width, the adsorption energies vary by less than 15 meV. ϵ_{diss} and ϵ_{ads} have been obtained within the static surface approximation consistently with what have been done in previous work[15].

The barriers for the direct dissociation ($E_b^{DirDiss}$) have been extracted from pre-computed 2D potential energy surfaces (PESs) in r and Z for different fixed impact sites and orientations. In the process of the indirect dissociation two barriers are involved (as shown in Figure 1): the first barrier separates the asymptotic configuration from the molecular adsorption state, while the second barrier separates the molecular adsorption state from the dissociative chemisorption state. The barriers for the molecular adsorption (E_b^{ent} or E_b^{Des} as referred to ϵ_{asym} or to ϵ_{ads}, respectively), see Figure 1, have been extracted from pre-calculated (r,Z) 2D PESs including the adsorption geometries. The barriers for the indirect dissociation (E_b^{ext} or $E_b^{IndDiss}$ as referred to ϵ_{asym} or to ϵ_{ads}, respectively) have been computed through climbing image nudged elastic band (CI-NEB) calculations. In the CI-NEB calculations, implemented in the VASP-TST package by Henkelman and Jónsson[30,31], four images have been optimized along the minimum energy path (MEP) between the reactants and the products. A CI-NEB calculation has been considered converged when the forces acting on all the images become smaller than 20 meV/Å. We tested this threshold by repeating one of the CI-NEB

calculations until the forces acting on all the images become smaller than 5 meV/Å and we found the same barrier height within 1 meV. We verified that the barrier geometries obtained with the CI-NEB calculations are real first-order saddle points by computing the vibrational frequencies.

In order to compute the reaction probability we performed ab initio molecular dynamics (AIMD) calculations[32–35]. AIMD allows one to model the N_2 + W(110) system while taking into account not only the six molecular degrees of freedom but also surface atom motion, which is known to considerably affect the dynamics of this system[15]. The AIMD trajectories have been propagated using the Verlet algorithm as implemented in VASP with a 1 fs time-step. Much of the details of our AIMD calculations are similar to those described in Ref.[15].

In order to compare our results with molecular beam experiments[7,8], which were performed for a surface temperature (T_s) of 800 K, the theoretical 0 K lattice constant has been multiplied with a factor 1.0037 in order to describe the experimental expansion of the bulk at 800 K[36]. For an optimal sampling of the surface initial conditions we equilibrated ten differently initialized W slabs. The initial displacements and velocities of the surface atoms have been generated according to an independent harmonic oscillators model. To overcome the harmonic approximation and achieve a proper description of the surface we next performed a 2.5 ps AIMD equilibration of the clean surfaces to impose the appropriate surface temperature. The surface initial conditions for the N_2 + W(110) trajectories have been randomly chosen from the last 1000 configurations assumed by the surfaces in the slab equilibrations, as described in Ref.[15]. To validate the 1 fs timestep we analyzed the total free energy (FE) through all our trajectories. For each trajectory the maximum variation of FE (ΔFE) is defined as:

$$\Delta\mathrm{FE} = \mathrm{FE}_{max} - \mathrm{FE}_{min} \tag{3}$$

where FE_{max} and FE_{min} are the maximum and the minimum value of FE during the evolution of the trajectory. In our simulations the total energy is conserved in almost all the trajectories with an average ΔFE around 25 meV and the number of trajectories in which the energy increases more than that is negligible.

In the molecule-surface dynamics the N_2 molecule is in the rovibrational ground-state (i.e. $v = 0$, $j = 0$), randomly oriented and placed with its center of mass (COM) 6 Å above the surface where the interaction potential is reasonably close to zero. A molecule has been considered scattered if, after the impact at the surface, the surface-molecule distance

becomes larger than 6 Å and the COM velocity is pointing away from the surface. A molecule is considered reacted if the interatomic distance (r) becomes larger than 2.0 Å (1.8 times the equilibrium interatomic distance) and if the distance between the two N atoms becomes larger than the distance between the first atom and the closest periodic image of the second atom. The reactive events have been classified as "direct" or "indirect" depending on whether the molecule performed, respectively, less than four or more than three rebounds on the surface before dissociating[10]. Consistently with previous work[15], one rebound has been counted every time the velocity of the molecule changes from pointing away from the surface to pointing towards the surface. The trajectories have been propagated until one of the described outcomes is found. However, in a few trajectories (between 6.5% and 4.5% of the total for the lowest E_i and normal and off-normal incidence, respectively, and in even fewer cases at higher E_i) the N_2 molecule remains trapped on the surface for a long time without either desorbing or dissociating. Because of the high computational cost of AIMD, in these cases the propagation has been stopped after 4.2 ps and the corresponding trajectories have been labeled as "unclear". A molecule has been considered trapped on the surface if it performed at least three bounces on the surface. The trapping probability has been defined as the number of trajectories in which the molecule undergoes trapping (regardless of the final outcome) divided by the total number of trajectories.

Each sticking probability value is estimated from 400 NVE trajectories (i.e. constant number of atoms, volume and total energy) performed for the same collision energy (E_i) and incidence angle (Θ_i) while including the N_2 zero-point energy in the calculation (quasi-classical trajectories, QCTs). For the scattered AIMD trajectories the amount of energy transferred to the surface (E_T) has been computed as:

$$E_T = (K + V)_{initial} - (K + V)_{final}, \tag{4}$$

by evaluating the kinetic energy of the molecule (K) and the interaction potential between the two N atoms (V) at the initial and at the final step of the trajectory. A positive value means that the energy is transferred from the molecule to the surface and a negative value means that the molecule takes energy from the surface. In equation 4 $K_{initial}$ and K_{final} are computed as the sum of the kinetic energies of the two N atoms in the first and in the last step of the dynamics, respectively. To obtain the potential energy terms we computed a fit of the one dimensional interatomic potential for the N_2 molecule and we obtained $V_{initial}$ and

V_{final} according to the interatomic N-N distance at the initial and at the final step of the dynamics respectively. Note that the energy transfer has been evaluated only for scattered molecules.

The relative variation of the interlayer distance Δd_{mn} with respect so the corresponding bulk value (d_b) has been defined as:

$$\Delta d_{mn} = (d_{mn} - d_b)/d_b, \tag{5}$$

where m and n a are indexes identifying the two layers considered. The results for T_S= 0 K, obtained by optimizing the slab interlayer distances while using the vdW-DF2 functional, show contraction of the first interlayer distance (i.e. Δd_{12} = -3.8 %) and a slight expansion of the second interlayer distance (i.e. Δd_{23} = 0.10 %) with respect so the corresponding bulk value (d_b). The same quantities obtained for T_S = 800 K, averaging over all the configurations employed for sampling the surface initial conditions, are not considerably different from the corresponding equilibrium values. However, Δd_{23} becomes negative in the dynamics picture. These results are in good agreement with previous theoretical work based on DFT with full-potential linearized augmented plane-waves (DFT-FLAPW)[37] and in reasonable agreement with X-ray diffraction experimental data[38] (Table I).

The reaction probabilities are reported with statistical error bars (σ_p) that represent the 68% confidence intervals[39]. For a reaction probability p calculated from the computation of N trajectories, σ_p is defined as:

$$\sigma_p = \sqrt{p(1-p)/N}. \tag{6}$$

The relative interlayer variations (Δd_{mn}) and the mean energy transfer from the molecule to the surface ($\langle E_T \rangle$) are reported with statistical standard errors (i.e., the standard deviation divided by the square root of the number of values used to compute the average).

III. RESULTS AND DISCUSSION

A. Static results

To properly model the dissociation of N_2 on W(110) a density functional that correctly describes the molecule-surface interaction is needed. Therefore we first studied the shape and

the features of the PES for molecular nitrogen interacting with an ideal W(110) surface, using the functional considered, through static calculations. The coordinate system employed is represented in Figure 2.

There is experimental[18,40] and theoretical[10,11,15,17] evidence for the existence of molecular adsorption states of N_2 on W(110). The associated configurations are believed to be relevant to the indirect dissociation mechanism in which the molecule remains trapped near the surface before dissociating[10,15]. The presence of deep molecular adsorption minima leads to an higher probability for the molecule to be trapped close to the surface and, therefore, an higher dissociation probability. As in previous work[15] three molecular adsorption geometries have been found; some details of these geometries are reported in Table II and a sketch of the molecular adsorption states is represented in Figure 3. The molecular adsorption states found are the following: the top-vertical (tpv) state, in which the molecule is perpendicular to the surface and above a top site, the hollow-parallel (hlp) state, in which the molecule is parallel to the surface with the center of mass above the four-fold hollow site (and $\phi = 0°$) and the bridge-hollow-tilted (bht) state, in which one of the two atoms is roughly above a bridge site and the other one close to an hollow site; in this geometry the molecular axis is neither perpendicular nor parallel to the surface.

The molecular adsorption energies (E_{ads}) for the adsorption states calculated with the vdW-DF2 functional are smaller than both the PBE and the RPBE values, with the exception of the top-vertical state for which E_{ads} is 0.1 eV larger (i.e., more negative) for the vdW-DF2 functional than for the RPBE functional (see Table III). E_{ads} for the bridge-hollow-tilted adsorption is particularly small (i.e. -0.286 eV, vs -0.984 eV for PBE and -0.543 eV for RPBE). Considering that the trapping mediated dissociation represents a large fraction of the reactivity at the lower E_i values investigated for PBE and RPBE and that for this collision energy range the experimental S_0 is overestimated with these functionals, the smaller values of E_{ads} found with the vdW-DF2 functional suggest a lower contribution of the indirect dissociation channel to the reactivity. As is shown in the next section, this does improve agreement with experimental data. For the vdW-DF functional the molecular adsorption energies calculated are very similar to the PBE results. Moreover previous static surface AIMD simulations performed by Martin-Gondre *et al.*[17] showed an underestimation of the experimental reaction probability using this functional. Therefore in this work we focus on the more promising vdW-DF2 functional. It is interesting that the tested vdW

functionals show generally weaker bonding for the molecular adsorption of N_2 but note that it is not easy to predict and to intuitively explain the behavior of a density functional. Moreover compared to the GGA functionals used (PBE and RPBE) both the exchange and the correlation parts change. The van der Waals functionals of the DF family (vdW-DF and vdW-DF2) have been designed to well reproduce purely vdW bond systems like rare gas dimers so they couple a non-local correlation term that accounts for vdW interaction with a repulsive GGA exchange (i.e., revPBE and rPW86 for the DF and for the DF2 functional respectively)[19,20]. This is one of the reasons of the short range repulsive nature of this functionals and makes them interesting for the aim of our study.

If a molecule approaches the surface at normal incidence, it may encounter an energy barrier[15] before reaching a molecular adsorption state. In order to investigate this, we computed two dimensional (r,Z) potential energy cuts setting the remaining degrees of freedom (DOF) equal to the ones characterizing the molecular adsorption geometries. The three elbow plots (Figure 3) have been computed interpolating (DFT) energy values on a fine grid in r and Z. The entrance channel barriers for molecular adsorption E_b^{ent} that are extracted from these 2D cuts are reported in Table IV together with the desorption barriers E_b^{Des}(calculated with respect to the bottom of the adsorption well). The vdW-DF2 barrier heights are intermediate between the PBE and the RPBE values, except for the access to the top-vertical state which is barrierless for the vdW-DF2 functional while small barriers were found for the PBE and the RPBE functionals (0.005 eV and 0.071 eV respectively). Two saddle points and two local minima have been found in the 2D plot corresponding to the hollow-parallel configuration. The first saddle point (black circle, Figure 3) is the E_b^{ent} barrier. We investigated the nature of the second 2D saddle point by means of geometry relaxation and frequencies calculations and we found than this is not a first order saddle point (i.e., a stationary point for which all the frequencies are real numbers except for one which is imaginary) in the full 6D space.

The vdW-DF2 functional has been developed to also model long-range attractive van der Waals interactions. To understand the properties of the PES far away from the surface, two one-dimensional energy diagrams have been computed (Figure 4). The bond length of N_2 has been fixed to the equilibrium value in the gas phase (i.e. 1.113 Å) and the molecule-surface interaction has been calculated varying the distance of the molecule's COM to the surface. Two potential curves have been computed for the molecule above the top site, one with the

molecular axis perpendicular and one with the molecular axis parallel to the surface. For Z>4 Å there is no potential difference between the two molecular orientations. For Z<4 Å a molecule perpendicular to the surface can enter the top-vertical adsorption well without any barrier, as mentioned above. At about 4 Å from the surface an adsorption well (vdW or physisorption well) of about 75 meV depth is observed in the vdW-DF2 results. Such a well is not observed with regular GGA functionals like PBE or RPBE.

In addition to the "straight paths" to access the molecular adsorption wells, a molecule could follow more complicated paths in which the impact site and the molecular orientation change along the path, potentially leading to lower barriers. For instance a molecule could follow a barrierless path to enter the top-vertical adsorption well and then move towards another adsorption state. CI-NEB calculations have been performed to obtain the MEPs and the barriers connecting the top-vertical adsorption state to the bridge-hollow-tilted and the hollow-parallel configuration. A small (18 meV) barrier has been found for the tpv-to-hlp path while the tpv-to-bht path is barrierless (Figure 5). Considering that the minimum translation energy of our AIMD trajectories is 0.9 eV the molecules should have always enough energy to overcome this small barrier and to explore the PES close to the surface without being confined in one of the molecular adsorption minima.

Previous work[10,15] showed that PBE overestimates the dissociation probability at E_i = 0.9 eV. Moreover, it was found[15] that the molecules that visit at least one of the molecular adsorption states dissociate in the majority of cases. These results would be consistent with the barriers for the dissociative chemisorption being too low compared to the ones for desorption from the molecular chemisorption well. Experimental work[18] also suggests that barriers for desorption and dissociation of similar height should be expected for N_2 on W(110). In fact, Lin *et al.*[18] studied N_2 on W(110) with different experimental techniques (temperature programmed desorption, Auger spectroscopy and X-ray photoelectron spectroscopy), estimating, for both the dissociation and the desorption, an activation energy of about 0.450 eV, which is reasonably similar to the barrier for the desorption from the top-vertical molecular adsorption state computed using vdW-DF2 (i.e. 0.480 eV).

Indirect dissociation barriers ($E_b^{IndDiss}$) and desorption barriers (E_b^{Des}) have been calculated using the vdW-DF2 functional. The latter have been extracted from the elbow plots in Figure 3 and the former have been calculated performing CI-NEB calculations connecting the molecular adsorption state to a dissociated configuration in which the N atoms are above

two bridge sites ("hollow-to-bridge" dissociation). The hollow-to-bridge geometry has been chosen as the final configuration of the CI-NEB calculations in order to simulate the dissociation above an hollow sites which is know to be involved in the dissociative chemisorption of N_2 on W(110)[10,15]. Moreover this geometry has been used as the final configuration of CI-NEB calculations on the same system in previous work[17]. The barrier heights, relative to the energy of the adsorption state (as illustrated in Figure 1), are reported in Table V A. The $E_b^{IndDiss}$ value for the path connecting the top-vertical molecular adsorption geometry and the hollow-to-bridge dissociation with the vdW-DF2 functional (marked with a dagger† in Table V) is extracted from Figure 2 of Ref.[17]. Note that this value was obtained allowing the relaxation of the two topmost surface layers in the NEB calculation whereas our results have been computed within the frozen surface approximation. Due to the very corrugated potential given by the vdW-DF2 functional has been impossible to converge the CI-NEB calculation to obtain the top-vertical dissociation barrier. Moreover Martin-Gondre et al.[17] found problems to obtain the barrier height for the same path within the frozen surface approximation. They managed to properly converge this path and to compute the barrier height only if the two topmost surface layers were allowed to relax. We reported this value in Table V. The exit channel barriers for the dissociation have also been calculated considering the asymptotic state as the energy zero (E_b^{ext}, reported in Table V B) and, for all the adsorption states and functionals, E_b^{ext} is negative (i.e. below the gas phase level). The vdW-DF2 functional shows lower desorption barriers than PBE and RPBE[15]; In general the values of $E_b^{IndDiss}$ and E_b^{Des} computed with vdW-DF2 are closer to each other than found with the other functionals, which is consistent with experimental results[18]. The better agreement of vdW-DF2 static results with the experimental findings suggests that, in the molecular dynamics simulation, there might be less indirect reaction, which could result in better agreement with the experimental reaction probability (S_0). As already noted, the vdW-DF2 barrier for the desorption from the top-vertical molecular adsorption state ($E_b^{Des} = 0.480$ eV) is in good agreement with the experimental barrier height suggested by Lin *et al.* (i.e., $\approx$0.450 eV). However, the vdW-DF2 barrier for the indirect dissociation is somewhat too low ($E_b^{IndDiss} = 0.406$ eV), it should be closer to the desorption barrier height.

Experimentally N_2 is known to adsorb on W(110) in a state which has been labeled γ-N_2 with an estimated adsorption energy of -0.450 eV[40]. This value agrees well with the adsorption energy we obtained with vdW-DF2 for the top-vertical adsorption state

(E_{ads} = -0.480 eV). There is also experimental evidence for another adsorption state of N_2 on W(110) called δ-N_2. Zhang et al.[40] reported the presence of this adsorption state generated through electron bombardment of γ-N_2 in electron stimulated desorption (ESD) experiments, and suggested an adsorption geometry with the molecule lying parallel to the surface with the N-N bond elongated with respect to N_2 in the gas-phase. The hollow-parallel adsorption state we found is characterized by a molecule placed parallel to the surface with an elongated N-N bond. Therefore, it might correspond to the experimentally observed δ-N_2 state. Moreover, the thermal programmed desorption (TPD) spectra before and after the ESD do not significantly differ, suggesting either that the desorption activation energy is similar for γ-N_2 and δ-N_2, or that the adsorbed molecules convert from the δ to the γ state before desorbing. Our findings are consistent with the latter explanation: in fact the hollow-parallel barrier for direct desorption (E_b^{Des} = 1.091 eV) is much higher than the barrier to convert the hollow-parallel adsorption state to the top-vertical adsorption state (E_b = 0.644 eV). However δ-N_2 has not been found to give rise to atomic N in TPD or ESD experiments, suggesting a large dissociation barrier for the δ-N_2 state, whereas the vdW-DF2 functional shows only a small dissociation barrier for the hollow-parallel state (i.e., $E_b^{IndDiss}$ = 0.182 eV).

We have studied the details of the energy landscape that influence the direct dissociation mechanism, which implies dissociation at the first impact on the surface or after a few rebounds. Four additional 2D cuts of the potential (Figure 6) have been computed considering four configurations that might be involved in this process. The configurations considered (Figure 7) involve the bridge-to-hollow dissociation, the bridge-to-hollow-shifted dissociation, the hollow-to-bridge dissociation, and the top-to-hollow dissociation. The first site specified in the configuration name is the the molecular COM position and the second one is the name of the site to which the two N atoms are pointing (for example, in the bridge-to-hollow configuration the center of mass is above a bridge site and the N atoms point towards two hollow sites). The configurations considered (Figure 7) are representative of all the possible 2D paths that allow the 2 N atoms to end up in two equivalent (local) adsorption minima (hollow, bridge, hollow-shifted) and the corresponding dissociative chemisorption energies (E_{diss}) are reported in Table VI. The real absolute atomic adsorption minimum is the one in which the N atoms are infinitely far from each other while, in our supercell, the real energy minimum is the one corresponding to the bridge-to-hollow-shifted dissociation.

The atomic adsorption site over the bridge site and the one over the hollow site are not real minima. They have been used as final configurations to simulate the dissociation above the hollow and the bridge sites respectively that are known to be relevant for this system. The E_{diss} values are calculated considering the asymptotic energy as energy zero and Table VI shows that the dissociative chemisorption of N_2 on W(110) is an exothermic process. The most stable dissociative geometry among the ones considered is the bridge-to-hollow-shifted geometry. The bridge-to-hollow and the top-to-hollow dissociation geometries differ in energy by 151 meV because the distances between the two N atoms differ in the dissociated geometries.

2D plots including the dissociation geometries mentioned above have been calculated with the same procedure as used for Figure 3. The barriers for the direct dissociation ($E_b^{DirDiss}$), as extracted from the 2D plots in Figure 6, are reported in Table VII. For the top-to-hollow dissociation we found a very high barrier at Z = 1.76 Å. For both the bridge-to-hollow and the hollow-to-bridge dissociation the MEP on the 2D PES shows two local minima and two saddle points. The entrance channel barriers for the direct dissociation ($E_b^{DirDiss}$, represented as black circles in Figure 6) are located in the region between 2.0 and 2.5 Å from the surface and the corresponding barrier heights, for vdW-DF2, are larger than for PBE but lower than for RPBE. Compared to RPBE, the vdW-DF2 functional is less repulsive far from the surface (Z > 2 Å) where the barriers for the direct dissociation are located. Performing geometry relaxation and frequencies calculations we verified that, in both cases, the first minimum along the MEP (between the two barriers) is not a real minimum in the 6D space for both hollow-to-bridge and bridge-to-hollow dissociation.

B. AIMD results

The reaction probability (S_0) has been computed for N_2 on W(110) for two incidence angles (Θ_i = 0° and 60°) and four initial collision energies (E_i = 0.90, 1.30, 1.70, 2.287 eV). We have compared AIMD results at normal incidence with the results of two molecular beam experiments of N_2 on W(110) performed at T_S = 800 K (Figure 8). The two experimental data sets, which were obtained by Pfnür *et al.*[8] and Rettner *et al.*[7], show a considerable difference in the reaction probability (Figure 8), in particular at high collision energies: for E_i = 2.3 eV the reaction probability obtained by Rettner *et al.* is about 0.1

smaller than the reaction probability obtained by Pfnür *et al.*. We found that multiplying the S_0 of Rettner *et al.* by a factor of 1.4 makes the reaction probability curve fall almost on top of the reaction probability curve obtained by Pfnür *et al.*. We focused the analysis of our results on the comparison with the Pfnür *et al.* results because their experiments, similarly to previous theoretical work[10,11,15], investigated both normal and off-normal incidence. Moreover Rettner *et al.*[7] did not give an explanation about the discrepancies between their sticking probabilities and the earlier results of Pfnür *et al.*[8].

For both incidence angles, the AIMD results are in good agreement with experimental data obtained by Pfnür *et al.*[8] at $E_i = 0.9$ eV but the agreement is less good for higher collision energies. For normal incidence the AIMD fails at reproducing the experimental trend: the experimental S_0 increases monotonically with E_i whereas the computed S_0 seems to show a minimum for E_i between 1.0 and 1.5 eV. For $\Theta_i = 60°$ the results are in good agreement with experiment at $E_i = 0.9$ eV, but at higher energies AIMD gives reaction probabilities that are three time smaller than the experimental ones. Compared to the data of Rettner *et al.*[7] for $\Theta_i = 0°$ the AIMD results are in quite good agreement with the experiments for $E_i = 2.287$ eV (Figure 8) while for lower collision energy (i.e., $E_i = 0.9$ eV) the AIMD results overestimate the Rettner *et al.* experimental reaction probability. Figure 8 also shows the upperbounds of the computed reaction probability obtained by considering all unclear trajectories as reacted. For the lowest E_i investigated the upperbound reaction probabilities are 0.065 and 0.045 larger than the regular ones for $\Theta_i = 0°$ and 60°, respectively. For higher E_i the upperbounds are not considerably different from S_0 and follow a similar trend in the dependence on E_i as the S_0 calculated in the regular way.

In Figure 9 vdW-DF2 AIMD results are also compared to previous calculations performed using PBE and RPBE (from Ref.[15]). For all E_i and incidence angles considered, the vdW-DF2 reaction probabilities are lower than the PBE results. Compared to RPBE, vdW-DF2 is less reactive for normal incidence. For $\Theta_i = 60°$, however, vdW-DF2 returns larger reaction probabilities for $E_i = 0.9$ eV but a similar reaction probability for $E_i = 2.3$ eV.

For the vdW-DF2 functional the indirect dissociation channel is still important at $E_i = 0.9$ eV, whereas at higher energies reactive events via trapping are rare for both $\Theta_i = 0°$ and 60° (Figure 10). For $\Theta_i = 0°$ vdW-DF2 indirect reaction probabilities are smaller than for both PBE and RPBE. For $\Theta_i = 60°$ vdW-DF2 indirect reaction probabilities are smaller than for PBE and larger than RPBE at E_i. Increasing the collision energy, the

vdW-DF2 reaction probability decreases, becoming smaller than for both PBE and RPBE. The vdW-DF2 direct reaction probability is always lower than for PBE. As noted before, for $\Theta_i = 60°$ the vdW-DF2 functional reproduces the experimental data of Pfnür *et al.*[8] well at the lowest E_i simulated but fails for higher energies where the direct dissociation mechanism dominates. One possibility is that this functional overestimates the barriers for direct dissociation returning a too low reaction probability at $E_i = 2.287$ eV.

The molecules that react indirectly at normal incidence spend considerable time bouncing on the surface before dissociating. Even for the direct reaction at the lower E_i values investigated and normal incidence, most of the molecules bounce at least once before the dissociation. This is not the case for $\Theta_i = 60°$ where the direct dissociation occurs mostly as soon as the molecule reaches the surface. Distributions of the COM positions and θ values, evaluated at the time of the dissociation (defined as the time at which the interatomic distance r becomes larger than 2 Å), are reported in Figures 11 and 12, respectively. Using the vdW-DF2 functional the direct reaction occurs at the hollow and bridge sites, while the indirect reaction occurs mostly at the hollow sites. Using the PBE and the RPBE functionals similar COM distributions are obtained for the direct and the indirect dissociation (not shown). The molecules react only when the axis is almost parallel to the surface ($\theta \approx 90°$) for both the direct and the indirect dissociation mechanisms (Figure 12).

The molecular trapping is related to the possibility, for the molecule, to lose its translational kinetic energy by transferring it to other molecular DOFs or to the surface. We evaluated the average amount of energy exchanged with the lattice ($\langle E_T \rangle$) for the scattering trajectories (Table VIII). For $\Theta_i = 0°$ a large portion of E_i is transferred to the lattice (i.e. 0.26 eV $< \langle E_T \rangle <$ 0.78 eV) whereas for $\Theta_i = 60°$ the energy transferred is smaller by about a factor two. Similar results have been found for PBE and RPBE[15]. Our results are also compared with the energy transfer predicted by the Baule model (E_T^{Baule}),[41] which approximates the molecule-surface impact as a collision between two hard-spheres with masses equal to the N_2 molecule and a target atom, which is typically taken as one of the surface atoms (i.e., a W atom):

$$E_T^{Baule} = E_i \frac{4\mu}{(1+\mu)^2}. \quad (7)$$

Here μ is the ratio between the mass of the N_2 molecule and the mass of one W surface atom. If the system considered shows a significant molecular adsorption energy, as for N_2 on W(110), the modified Baule model is generally used to take into account the additional

kinetic energy that the projectile gains approaching the surface. In the modified Baule model E_i is substituted by (E_i + E_{ads}) where E_{ads} is the adsorption energy (in our case we used the largest adsorption energy, which is the one related to the hollow-parallel configuration, i.e. E_{ads}=0.626 eV). Table VIII reports the energy transfer values computed with the Baule model (Table VIII A) and the values computed from the average over the AIMD scattered trajectories (Tables VIII B and VIII C).

We also compared the energy exchanged by the molecules that scattered after a single impact on the surface ($\langle E_T \rangle_1$) with the Baule model predictions (Figure 13), showing that the Baule model considerably overestimates the amount of energy transferred to the surface even considering a single molecule-surface collision.

For PBE and RPBE[15] a large fraction of the molecules undergo molecular trapping (between 15 and 40%, depending on E_i and Θ_i) as also reported in Figure 14. Most of the trapped molecules end up dissociating. For vdW-DF2 we found that the fraction of the trajectories that involve molecular trapping (between 0.05 and 0.2) is significantly lower than for the other functionals at $\Theta_i = 0^\circ$ (Figure 14). For $\Theta_i = 60^\circ$ the fraction of trapped molecules found with vdW-DF2 is smaller than for PBE and monotonically decreases with increasing collision energy (Figure 14). On average, 60% of the trapped molecules dissociate (Figure 15). As found for PBE and RPBE[15], for normal incidence the fraction of trapped molecules that dissociate is independent of the collision energy. For $\Theta_i = 60^\circ$ it is not possible to identify a clear trend because the statistics are poor due to the low number of trapped trajectories at this incidence angle (Figure 15).

Some trajectories are still trapped on the surface at the end of the propagation time (i.e., 4200 fs) without a clear outcome (reaction or scattering). 80% of the reactive events occur before a propagation time t'=1600 fs (roughly 40% of our maximum propagation time) and all the molecules that dissociate after that time go through the indirect dissociation channel. If we assume the ratio between the molecule scattered and dissociated after t' to be constant in time, we can extrapolate dissociation probabilities for larger propagation times assigning an outcome to the unclear trajectories. The two S_0 points associated with the highest number of unclear trajectories are at E_i = 0.9 eV for both $\Theta_i = 0^\circ$ and 60° and they show a reaction/desorption ratio after t' of 1.25 and 0.56, respectively. If an outcome is assigned to the unclear trajectories according to this extrapolation the computed S_0 values would increase by 0.036 for E_i = 0.9 eV and $\Theta_i = 0^\circ$ and by 0.016 for E_i = 0.9 eV and Θ_i

= 60°. The main conclusions of our work would not change on the basis of these estimates, and the small increase of the reaction probability due to this extrapolation shows that the upperbounds to the reaction probabilities reported in Figure 8 are probably somewhat too large.

The long range van der Waals interaction (Figure 4) directly affects the dynamics through the introduction of a shallow molecular adsorption (physisorption) well. Note that this physisorption well is not present if traditional functionals like PBE and RPBE are employed, as regular GGA functionals fail to describe long-range dispersion interaction. A molecule can be trapped either in one of the molecular adsorption (chemisorption) minima previously described (at Z≈3 Å from the surface) or in the vdW well (at Z between 3.5 and 5 Å from the surface). To illustrate the two kinds of adsorption we have chosen two representative trajectories (Figure 16). In Figure 16 D the kinetic energy along the surface normal is plotted as a function of time for a molecule trapped in the vdW well (reported in red) and for a molecule trapped close to the surface (reported in green). We observe trapping in the vdW well only following the molecule-surface collision: it is only through the impact with the surface that the high collision energy can be transferred from the Z degree of freedom to other molecular or surface DOFs, allowing for the trapping in the shallow vdW well. Due to the low corrugation of the potential and the large distance from the surface, energy exchange between the molecular and the molecule-surface DOFs is expected to be slow. Therefore the dissociation of a molecule trapped in the vdW well might occur on a time scale that is too large compared to what can be afforded with the AIMD method. However, using the vdW-DF2 functional, the trapping in the vdW well is quite rare at the collision energies investigated: for $\Theta_i = 0°$ we found that only 3% of the trajectories undergo trapping in the vdW well, and this value decreases to zero for higher collision energies and angles (Figure 16 A). Therefore, assigning an outcome to these trajectories would not considerably change the conclusions of this work.

IV. SUMMARY AND CONCLUSIONS

In this work, we have studied the static properties of the PES and we have computed the sticking probability for N_2 on W(110) employing AIMD. All the electronic structure calculations have been performed using functionals that include long range van der Waals

interactions, as already tested on this system by Martin-Gondre *et al.*[17] with static and dynamic calculation, but only within the ideal and frozen surface approximation. We extended the static study for the vdW-DF and the vdW-DF2 functionals considering more molecular adsorption configurations and we performed AIMD calculations, testing the vdW-DF2 functional, accounting for surface atom motion effects and long range interactions.

Using the vdW-DF2 functional, the PES shows improvements compared to standard GGA functionals like PBE and RPBE[15]. The molecular adsorption wells are less deep and the barriers for the indirect dissociation and for the desorption from these molecular adsorption states are more similar to each other than with the semi-local functionals, in better agreement with experimental evidence[18]. Using the vdW-DF2 functional, the AIMD simulations show a lower trapping-mediated reaction probability than found for PBE and RPBE[15], resulting in a reasonable agreement with the molecular beam experiments of Pfnür *et al.*[8] at $E_i = 0.9$ eV.

However, AIMD underestimates the reaction probability measured by Pfnür *et al.* at the higher E_i values investigated, where the trapping-mediated dissociation mechanism is negligible, resulting in a dissociation probability curve that does not depend on E_i, as previously found with semi-local functionals modeling surface atom motion[15]. This seems to suggest that the vdW-DF2 functional is still too repulsive in the area of the PES far from the surface in spite of the attractive vdW interaction modeled, and that the barriers for direct dissociation computed with the vdW-DF2 functional might still be too high.

ACKNOWLEDGMENTS

This work was made possible by the financial support from the European Research Council through an ERC-2013 advanced grant (Nr. 338580) and by the Nederlandse Organisatie voor Wetenschappelijk Onderzoek (Netherlands Organization for Scientific Research, NWO). The authors also acknowledge NWO Exacte Wetenschappen, EW (NWO Physical Science Division) for granting access to the Cartesius supercomputer and to the Lisa computer cluster.

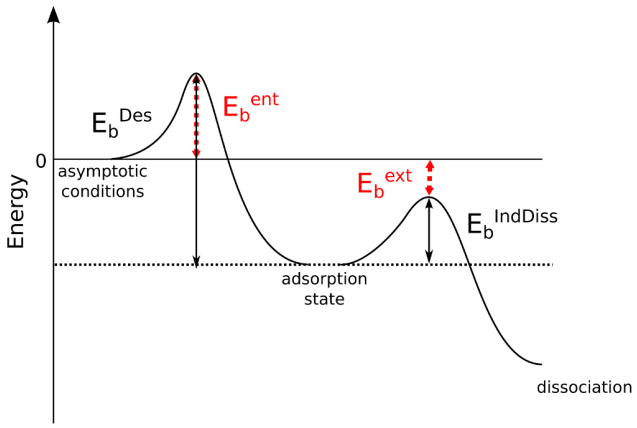

Figure 1. Scheme of the barriers considered. The barrier for the desorption (E_b^{Des}) and the barrier for the indirect dissociation ($E_b^{IndDiss}$), represented as thick black lines are referred to the energy of the adsorption state. The entrance channel barrier for the molecular adsorption (E_b^{ent}) and the exit channel barrier for the dissociative chemisorption (E_b^{ext}), represented as red dash lines, are referred to the asymptotic energy.

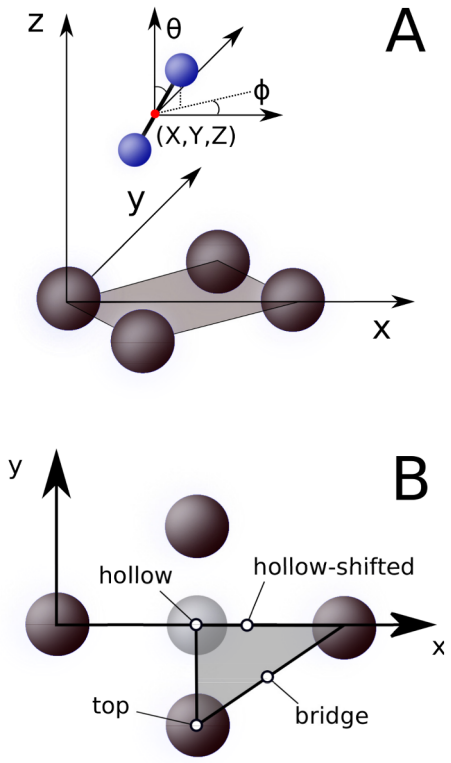

Figure 2. Coordinate system (A) and sites on the surface (B). Dark gray, light gray and blue are used for first layer W atoms, second layer W atoms and nitrogen respectively. In figure A, the coordinates of the molecular center of mass are reported (X,Y,Z). In figure B the irreducible wedge is indicated.

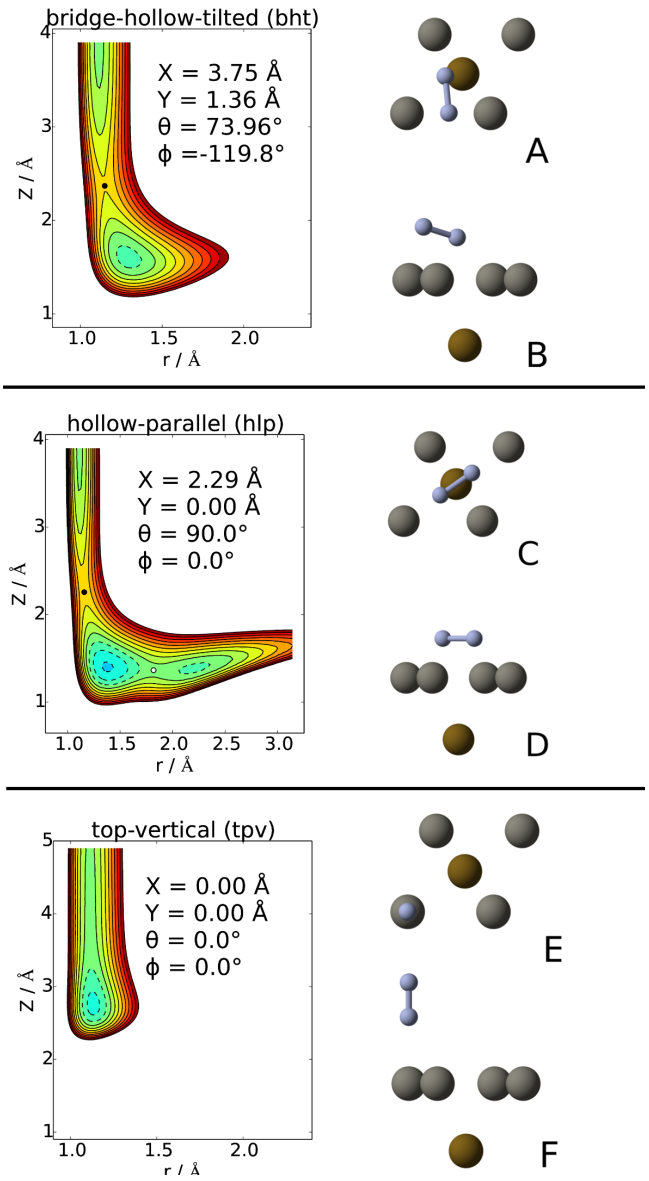

Figure 3. Left: 2D (r,Z) cuts of the PES computed for the three molecular adsorption geometries. Contour lines separate 0.2 eV energy intervals, solid lines are used for E $\geq$ 0 eV while dashed lines for E $<$ 0 eV. Circles indicate all the (first order) saddle points. The black circles represent the entrance channel barriers for molecular adsorption (E_b^{ent}) and the white circles are 2D saddle-points that are not real first order saddle-points in the 6D space (see text for details). Some details about the molecular adsorption geometries considered are reported as insets in the related plots. Right: top view (A, C, E) and side view (B, D, F) of the adsorption states. bridge-hollow-tilted (A,B), hollow-parallel (C,D) and top-vertical adsorption (E,F) are shown. The first layer atoms are shown in gray and the second layer atom closest to the molecule is shown in brown, the nitrogen atom are shown in blue (the acronyms used denoting the adsorption states geometries are defined in the text).

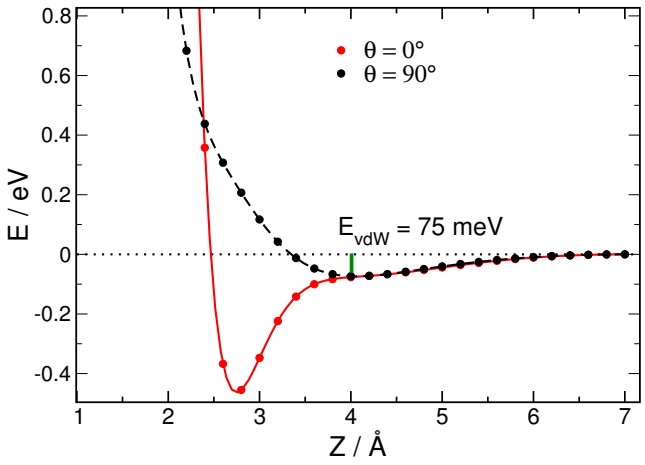

Figure 4. 1D cuts of the potential as a function of the distance between the molecule's COM from the surface (Z) above a top site oriented either parallel ($\theta = 90°$) or perpendicular ($\theta = 0°$) to the surface. The zero of energy is the absolute energy of the molecule in the asymptotic configuration at gas phase equilibrium intramolecular distance ($r = r_e$).

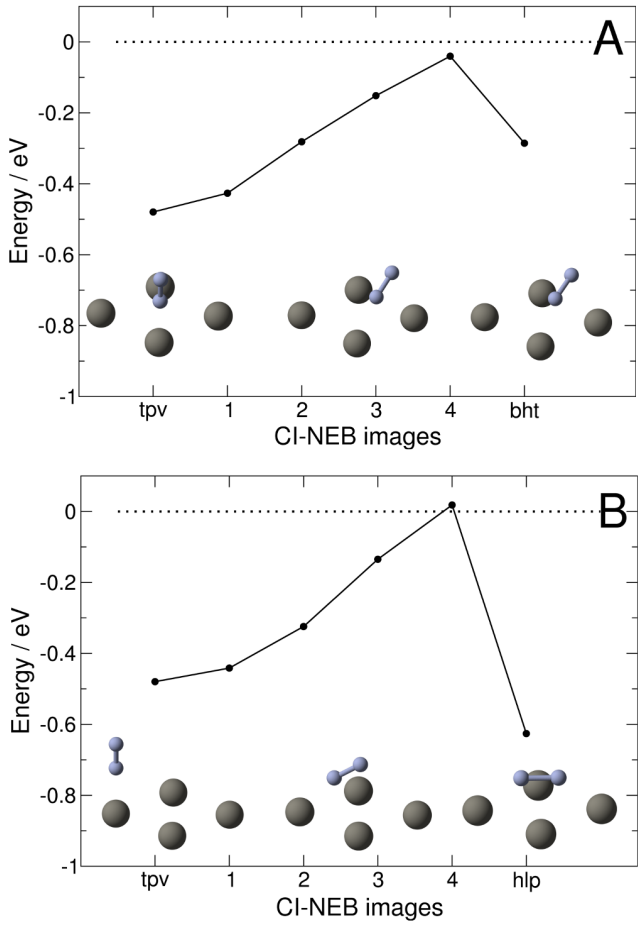

Figure 5. Paths connecting two molecular adsorption states as obtained from CI-NEB calculations. The paths connect the top vertical state to either the bridge hollow tilted (A) or to the hollow parallel state (B). The zero of energy is the absolute energy of the molecule in the asymptotic configuration. The initial, the barrier and the final geometries are sketched as insets in the plots.

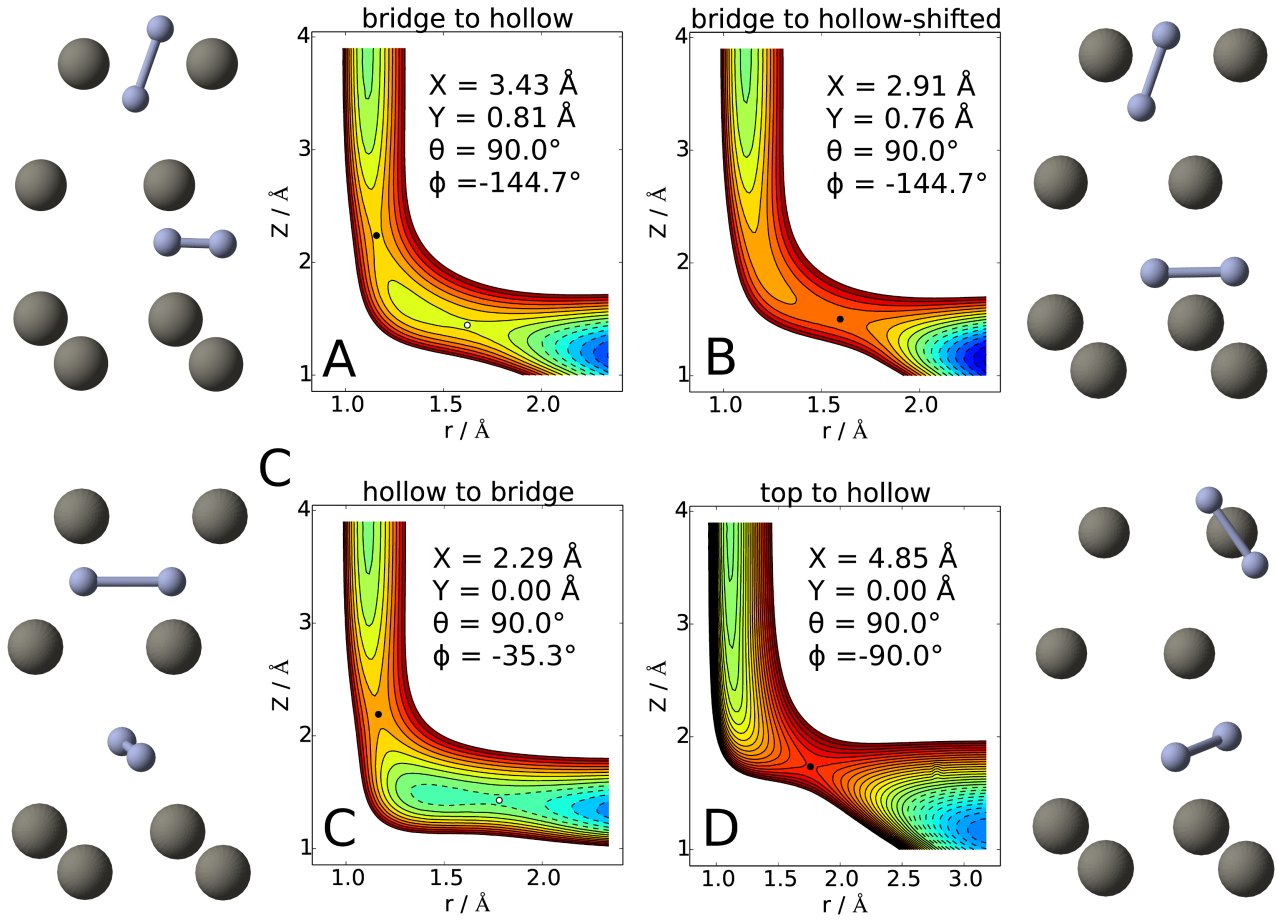

Figure 6. 2D (r,Z) cuts of the PES computed for four dissociation geometries: bridge-to-hollow (A), bridge-to-hollow-shifted (B), hollow-to-bridge (C) and top-to-hollow (D). Contour lines separate 0.2 eV energy intervals, solid lines are used for E $\geq$ 0 eV and dashed lines for E $<$ 0 eV. Circles indicate all the stationary points. The black circles represent the entrance channel barriers for dissociation ($E_b^{DirDiss}$) and the white circles are 2D saddle-points that are not real first order saddle-points in the 6D space (see text for details). The top and the side view sketches of the direct dissociation barrier geometries are reported next to the corresponding elbow plots.

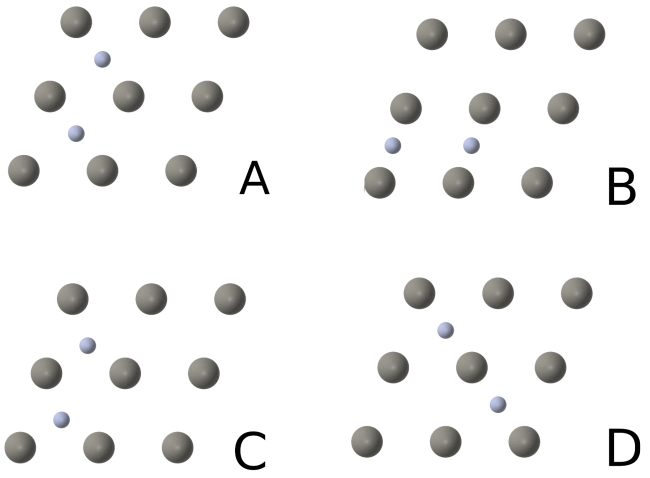

Figure 7. Dissociation products considered as a result of a bridge-to-hollow (A), hollow-to-bridge (B), bridge-to-hollow-shifted (C) and top-to-hollow (D) dissociation.

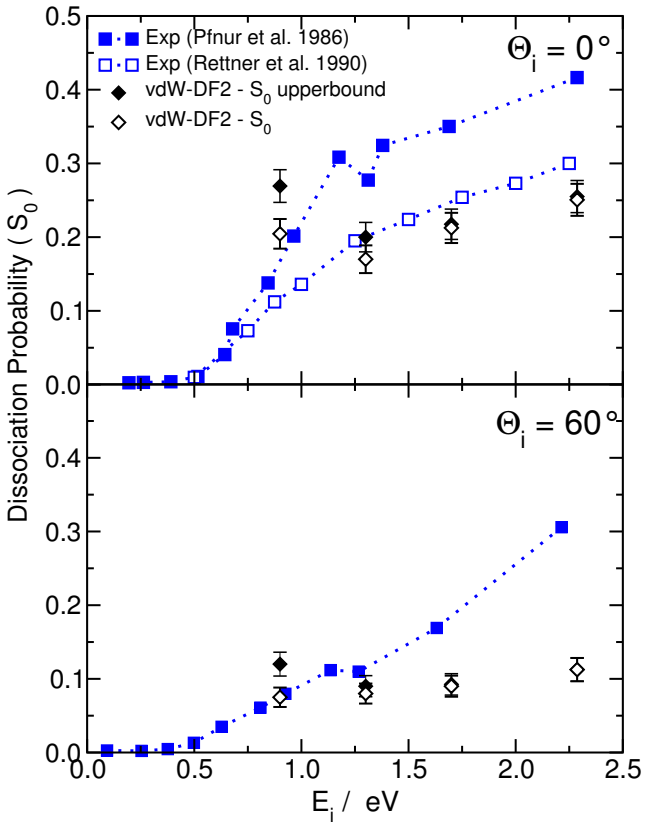

Figure 8. Reaction probability as a function of the collision energy E_i for Θ_i=0° (top panel) and Θ_i=60° (bottom panel). Comparison between experimental data and AIMD vdW-DF2 results. The dissociation probabilities and their upperbounds are reported as empty and full black symbols, respectively. Experimental data are taken from Ref.[7] (full blue symbols) and Ref.[8] (empty blue symbols).

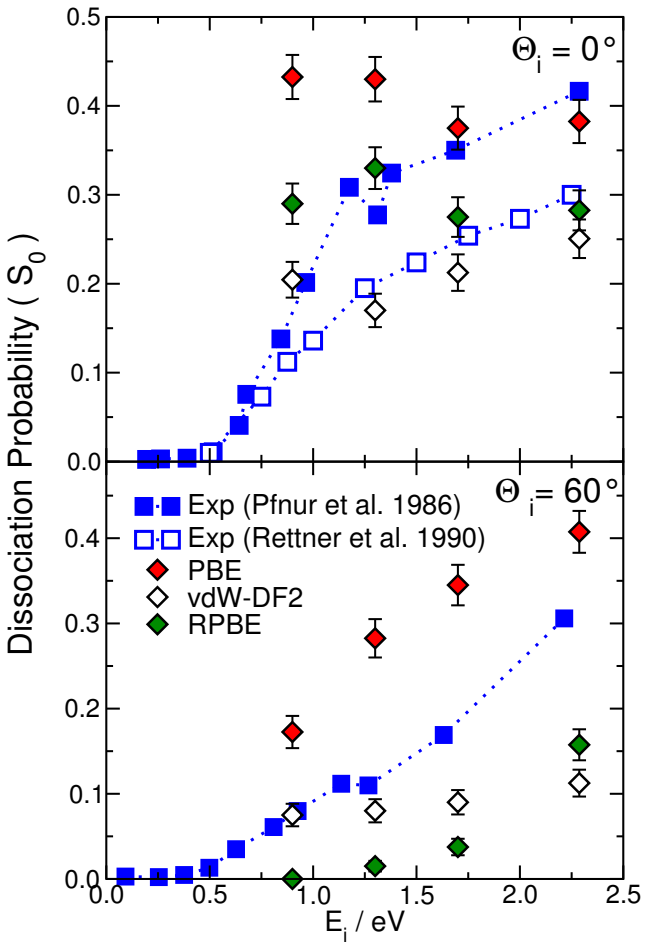

Figure 9. Reaction probability as a function of the collision energy E_i for Θ_i=0° (top panel) and Θ_i=60° (bottom panel). vdW-DF2 results are reported as black empty diamonds. PBE and RPBE data (full red and green diamonds, respectively) for normal incidence are taken from Ref.[15]. Experimental data are taken from Ref.[7] (full blue squares) and Ref.[8] (empty blue squares).

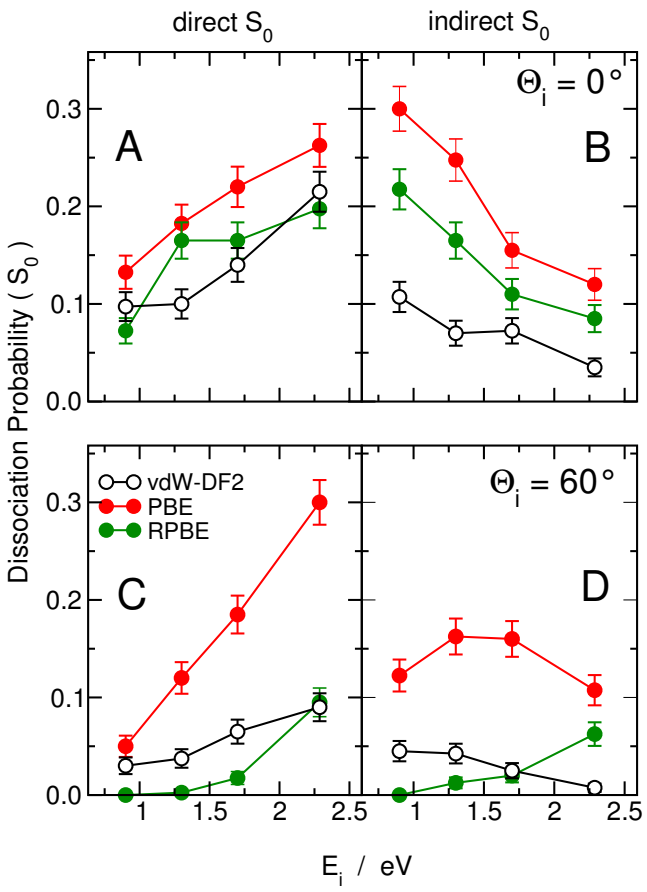

Figure 10. Direct (A,C) and indirect (B,D) reaction probability as a function of E_i for Θ_i=0° (A,B) and Θ_i=60° (C,D). vdW-DF2 results are reported as black empty circles. PBE and RPBE data (full red and green circles, respectively) for normal incidence are taken from Ref.[15].

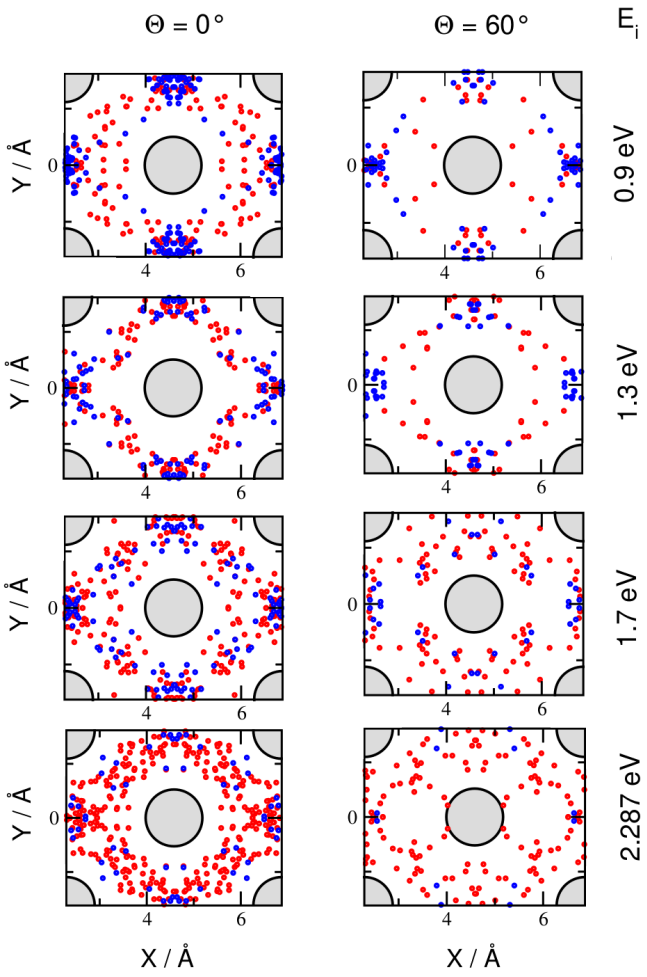

Figure 11. XY position of the COM of the reactive molecules at the time of the dissociation (see text for definition). The COM positions have been reported in the minimum wedge and then replicated in the $\sqrt{2}$x$\sqrt{2}$ super-cell using symmetry operations. Direct and indirect events are indicated as red and blue circles respectively. Tungsten first layer atoms in their equilibrium positions are shown as gray circles.

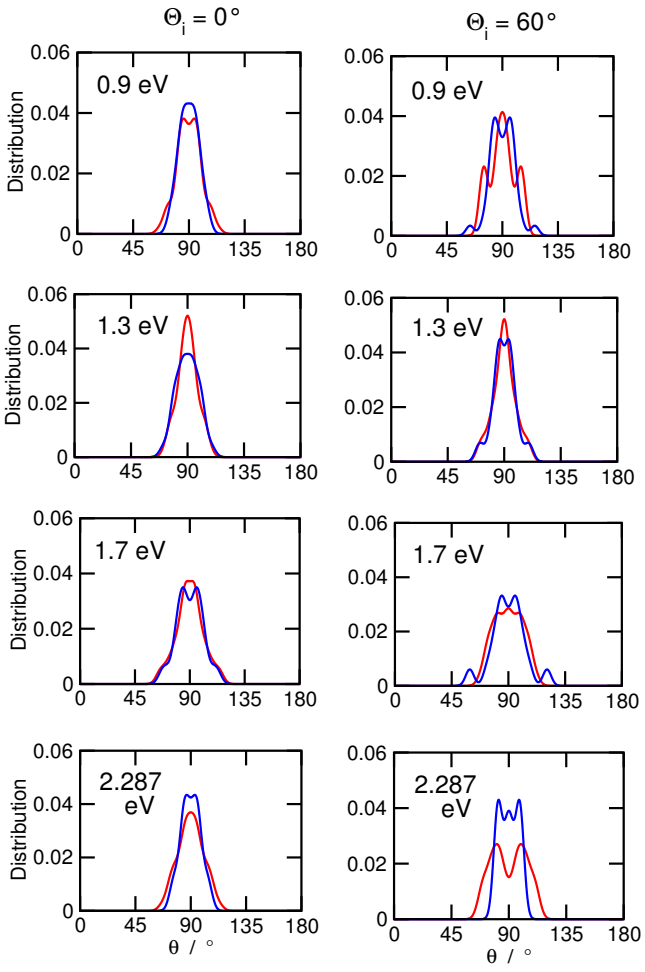

Figure 12. Distribution of the angle between the molecular axis and the surface normal (θ) at the time of the reaction (see text for definition) for both the direct and the indirect mechanisms (red and blue lines, respectively). To increase the resolution of the data, for each molecule have been reported the two values of θ obtained inverting the N atoms (i.e., the angles θ and $180° - \theta$ have been reported for each atom). The incidence energy E_i is reported as inset.

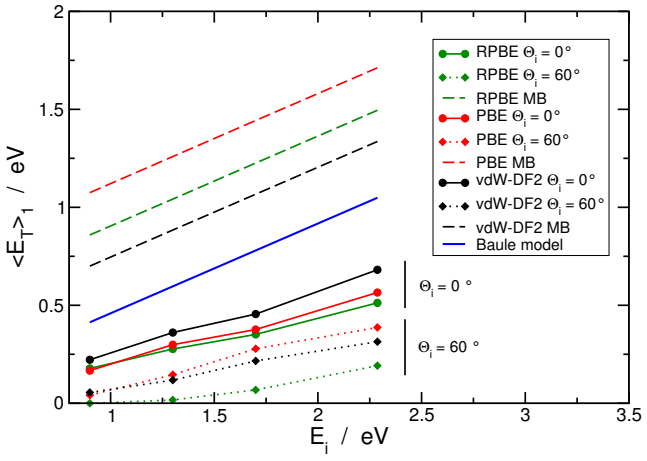

Figure 13. Comparison between the mean energy transfer to the surface calculated from the molecules that do not perform any rebounds on the surface ($\langle E_T \rangle_1$) and the energy transfer predicted by the modified Baule model. Data are reported for the functionals considered (in red, green, and black, for PBE, RPBE and vdW-DF2, respectively) for Θ_i=0° (solid lines), Θ_i=60° (dotted lines) and for the modified Baule model (dashed lines). The standard Baule model is reported as a thick blue line. PBE and RPBE data are taken from Ref.[15].

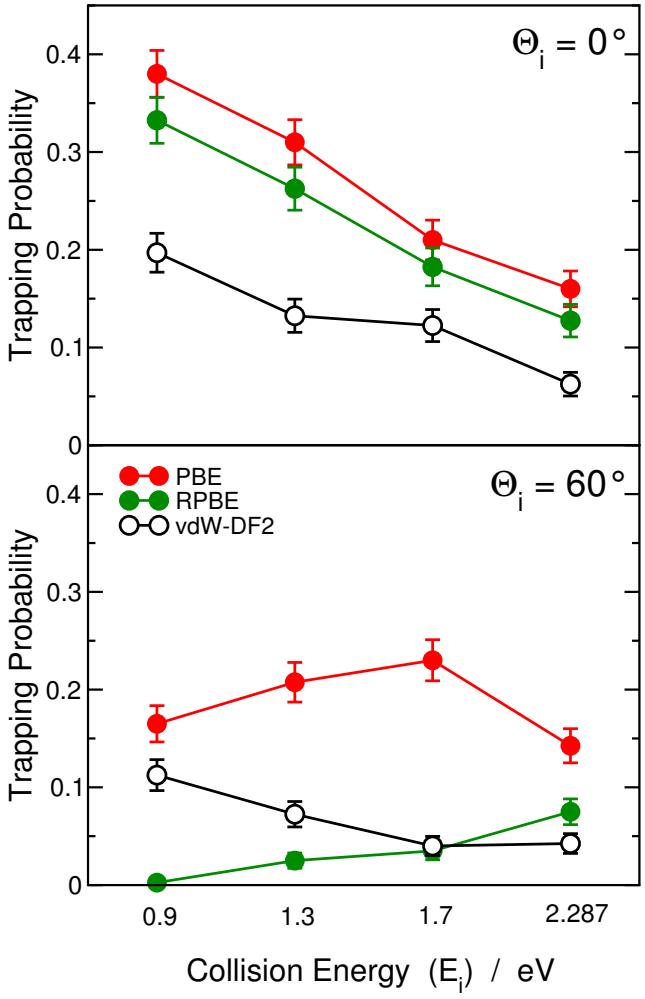

Figure 14. Comparison between the trapping probabilities computed with the PBE, RPBE and vdW-DF2 functional (reported as full red, full green and empty black circles respectively) for both $\Theta_i = 0°$ (top panel) and $\Theta_i = 60°$ (bottom panel).

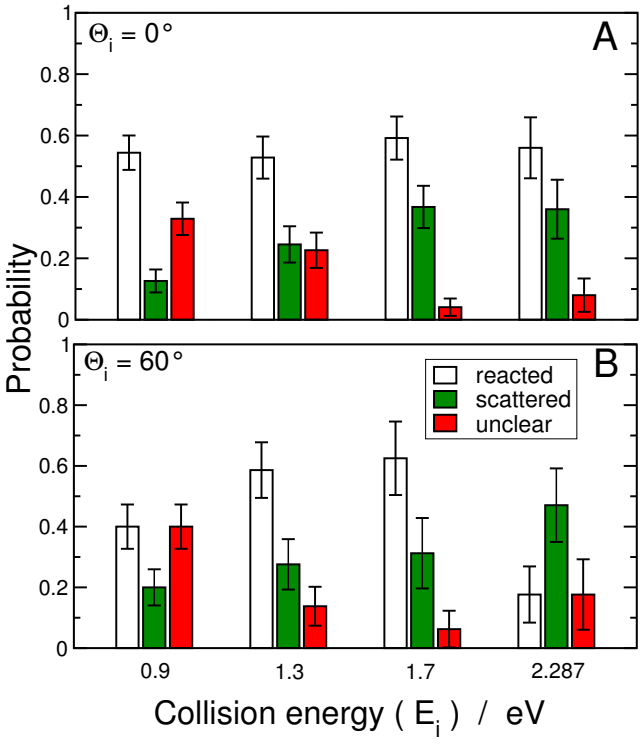

Figure 15. The white, green and red bars represent the probabilities for a trapped molecule to dissociate, to scatter or to remain trapped (unclear outcome), respectively. The result reported are for $\Theta_i = 0°$ (panel A) and $\Theta_i = 60°$ (panel B).

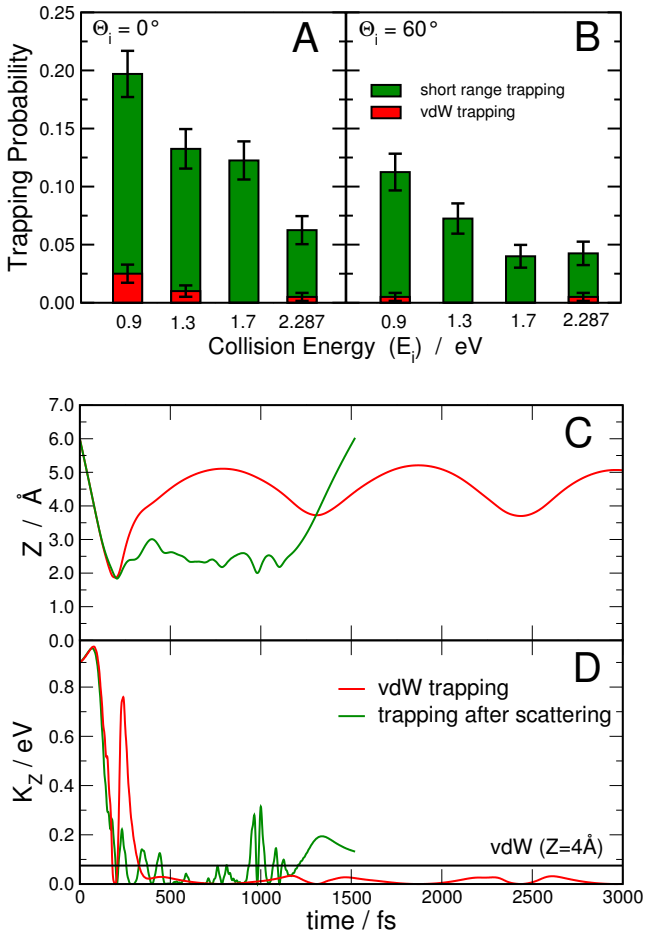

Figure 16. (A, B) Probability of short range and vdW trapping for the collision energies and angles studied. (C, D) Comparison between two trajectories undergoing short-range (green) and vdW (red) trapping; the distance from the surface (Z) and the kinetic energy along Z (K_Z) are plotted as a function of time. In panel (D), the interaction potential calculated at Z=4 Å is plotted as an horizontal black line.

	vdW-DF2 T_s=0 K (equilibrium)	vdW-DF2 T_s=800 K (dynamics)	DFT-FLAPW[37]	X-ray diffraction[38]
Δd_{12}	-4.20 %	-4.10 ± 0.02 %	-4.1 %	-2.7 ± 0.5 %
Δd_{23}	0.10 %	-0.96 ± 0.02 %	-0.4 %	0.0 ± 0.3 %

Table I. Relative interlayer variations with respect to the bulk computed from experiments and with different theoretical methods.

		θ / °	r / Å	Z / Å
PBE	tpv	0.00	1.137	2.672
	hlp	90.00	1.363	1.378
	bht	74.48	1.307	1.537
RPBE	tpv	0.00	1.141	2.694
	hlp	90.00	1.370	1.391
	bht	74.61	1.316	1.544
vdW-DF	tpv	0.00	1.141	2.707
	hlp	90.00	1.395	1.397
	bht	74.79	1.330	1.560
vdW-DF2	tpv	0.00	1.130	2.744
	hlp	90.00	1.375	1.402
	bht	73.96	1.290	1.598

Table II. Molecular adsorption geometries as obtained with different functionals. Z is the distance between the center of mass (COM) of the molecule and the surface, r is the N-N distance and θ is the polar angle of orientation of the molecule. The tpv, hlp and bht abbreviations stand for top-vertical, hollow-parallel and bridge-hollow-tilted respectively. The PBE and the RPBE data are from Ref.[15].

	E_{ads}		
	tpv	hlp	bht
PBE	-0.621	-1.444	-0.984
RPBE	-0.385	-0.972	-0.543
vdW-DF	-0.661	-1.340	-0.904
vdW-DF2	-0.480	-0.626	-0.286

Table III. Molecular adsorption energies for N_2 on W(110), in eV. The tpv, hlp and bht abbreviations stand for top-vertical, hollow-parallel and bridge-hollow-tilted respectively. The PBE and the RPBE data are from Ref.[15].

	E_b^{ent} (E_b^{Des})		
	tpv	hlp	bht
PBE	0.005 (0.626)	0.406 (1.850)	0.387 (1.371)
RPBE	0.071 (0.456)	0.629 (1.601)	0.610 (1.153)
vdW-DF2	- (0.480)	0.465 (1.091)	0.405 (0.691)

Table IV. Entrance channel barriers for molecular adsorption (E_b^{ent}) and for the desorption (E_b^{Des}, in brackets), in eV. The tpv, hlp and bht abbreviations stand for top-vertical, hollow-parallel and bridge-hollow-tilted respectively. All the vdW-DF2 values are extracted from the 2D cuts in Figure 3, the PBE and the RPBE data are from Ref.[15].

	tpv		hlp		bht	
	$E_b^{IndDiss}$	E_b^{Des}	$E_b^{IndDiss}$	E_b^{Des}	$E_b^{IndDiss}$	E_b^{Des}
PBE	0.189	0.626	0.467	1.850	0.498	1.371
RPBE	0.271	0.456	0.442	1.601	0.500	1.153
vdW-DF2	0.406†	0.480	0.182	1.091	0.271	0.691

(A)

	tpv		hlp		bht	
	$E_b^{IndDiss}$	E_b^{ext}	$E_b^{IndDiss}$	E_b^{ext}	$E_b^{IndDiss}$	E_b^{ext}
PBE	0.189	-0.432	0.467	-0.977	0.498	-0.486
RPBE	0.271	-0.114	0.442	-0.550	0.500	-0.043
vdW-DF2	0.406†	-0.170†	0.182	-0.444	0.271	-0.015

(B)

Table V. (A) Barriers (in eV) for the desorption (E_b^{Des}) and for the dissociation ($E_b^{IndDiss}$) as calculated from the bottom of the molecular adsorption wells indicated. (B) Comparison between the dissociation barriers (in eV) calculated with respect to the asymptotic configuration (E_b^{ext}) or with respect of the bottom of the molecular adsorption configuration indicated ($E_b^{IndDiss}$). The tpv, hlp and bht abbreviations stand for top-vertical, hollow-parallel and bridge-hollow-tilted respectively. The PBE and the RPBE data are from Ref.[15]. The $E_b^{IndDiss}$ and E_b^{ext} values for tpv, marked with a dagger (†), are extracted from Figure 2 of Ref.[17]. Note that these values were obtained allowing the relaxation of the two topmost surface layers in the NEB calculation whereas the other results have been computed within the frozen surface approximation, see text for details.

configuration	E_{diss} / eV
hollow-to-bridge	-1.273
bridge-to-hollow	-1.848
top-to-hollow	-1.999
bridge-to-hollow-shifted	-2.445

Table VI. Dissociation energies (in eV) of the dissociated configurations sketched in Figure 7.

	$E_b^{DirDiss}$			
	hollow-to-bridge	bridge-to-hollow	top-to-hollow	bridge-to-hollow-shifted
PBE	0.543	0.487	-	-
RPBE	0.802	0.726	-	-
vdW-DF2	0.635	0.563	2.612	0.881

Table VII. Barriers for the direct dissociation (in eV) extracted from the elbow plots in Figure 6. The PBE and the RPBE data are from Ref.[15].

E_i (eV)	Baule (eV)	Modified Baule (eV)		
		vdW-DF2	PBE	RPBE
0.900	0.413	0.700	1.075	0.859
1.300	0.596	0.884	1.259	1.042
1.700	0.780	1.067	1.443	1.226
2.287	1.049	1.336	1.712	1.495

(A)

$\Theta_i = 0°$

	$\langle E_T \rangle$ (eV)		
E_i	vdW-DF2	PBE	RPBE
0.900	0.257 ± 0.001	0.214 ± 0.012	0.210 ± 0.011
1.300	0.396 ± 0.002	0.348 ± 0.016	0.335 ± 0.014
1.700	0.546 ± 0.002	0.483 ± 0.022	0.450 ± 0.019
2.287	0.779 ± 0.001	0.654 ± 0.022	0.623 ± 0.022

(B)

$\Theta_i = 60°$

	$\langle E_T \rangle$ (eV)		
E_i	vdW-DF2	PBE	RPBE
0.900	0.104 ± 0.001	0.071 ± 0.008	0.002 ± 0.002
1.300	0.183 ± 0.001	0.225 ± 0.016	0.005 ± 0.006
1.700	0.280 ± 0.001	0.414 ± 0.022	0.011 ± 0.011
2.287	0.388 ± 0.001	0.546 ± 0.028	0.019 ± 0.019

(C)

Table VIII. (A) Energy transfer to the surface according to the Baule model and the modified Baule model (see text for details) for the E_i considered. (B, C) The mean energy transfer $\langle E_T \rangle$ computed averaging over the scattered trajectories is reported for all the functionals and collision energies for Θ_i=0° and Θ_i=60°. PBE and RPBE data are taken from Ref.[15].

REFERENCES

[1]A. Nilsson, L. G. M. Pettersson, and J. K. Nørskov (Eds.), *Chemical Bonding at Surfaces and Interfaces* (Elsevier, Amsterdam, 2008).

[2]G. A. Somorjai and Y. Li, Proc. Natl. Acad. Sci. U. S. A. **108**, 917 (2011).

[3]G. Ertl, Catal. Rev. **21**, 201 (1980).

[4]F. Bozso, G. Ertl, M. Grunze, and M. Weiss, J. Catal. **49**, 18 (1977).

[5]S. P. Singh-Boparai, M. Bowker, and D. A. King, Surf. Sci. **53**, 55 (1975).

[6]C. T. Rettner, H. Stein, and E. K. Schweizer, J. Chem. Phys. **89**, 3337 (1988).

[7]C. T. Rettner, E. K. Schweizer, and H. Stein, J. Chem. Phys. **93**, 1442 (1990).

[8]H. E. Pfnür, C. T. Rettner, J. Lee, R. J. Madix, and D. J. Auerbach, J. Chem. Phys. **85**, 7452 (1986).

[9]M. Alducin, R. Díez Muiño, H. F. Busnengo, and A. Salin, Phys. Rev. Lett. **97**, 056102 (2006).

[10]M. Alducin, R. Díez Muiño, H. F. Busnengo, and A. Salin, J. Chem. Phys. **125**, 144705 (2006).

[11]G. A. Bocan, R. Díez Muiño, M. Alducin, H. F. Busnengo, and A. Salin, J. Chem. Phys. **128**, 154704 (2008).

[12]J. P. Perdew, J. A. Chevary, S. H. Vosko, K. A. Jackson, M. R. Pederson, D. J. Singh, and C. Fiolhais, Phys. Rev. B **46**, 6671 (1992).

[13]J. P. Perdew, J. A. Chevary, S. H. Vosko, K. A. Jackson, M. R. Pederson, D. J. Singh, and C. Fiolhais, Phys. Rev. B **48**, 4978 (1993).

[14]B. Hammer, L. B. Hansen, and J. K. Nørskov, Phys. Rev. B **59**, 7413 (1999).

[15]F. Nattino, F. Costanzo, and G. J. Kroes, J. Chem. Phys. **142**, 104702 (2015).

[16]J. P. Perdew, K. Burke, and M. Ernzerhof, Phys. Rev. Lett. **77**, 3865 (1996).

[17]L. Martin-Gondre, J. I. Juaristi, M. Blanco-Rey, R. Díez Muiño, and M. Alducin, J. Chem. Phys. **142**, 074704 (2015).

[18]J. C. Lin, N. Shamir, Y. B. Zhao, and R. Gomer, Surf. Sci. **231**, 333 (1990).

[19]M. Dion, H. Rydberg, E. Schröder, D. C. Langreth, and B. I. Lundqvist, Phys. Rev. Lett. **92**, 246401 (2004).

[20]K. Lee, É. D. Murray, L. Kong, B. I. Lundqvist, and D. C. Langreth, Phys. Rev. B **82**, 081101 (2010).

[21]G. J. Kroes, J. Phys. Chem. Lett. **6**, 4106 (2015).

[22]G. Kresse and J. Hafner, Phys. Rev. B **47**, 558 (1993).

[23]G. Kresse and J. Furthmüller, Comput. Mater. Sci **6**, 15 (1996).

[24]G. Kresse and J. Furthmüller, Phys. Rev. B **54**, 11169 (1996).

[25]G. Kresse and D. Joubert, Phys. Rev. B **59**, 1758 (1999).

[26]P. E. Blöchl, Phys. Rev. B **50**, 17953 (1994).

[27]G. Román-Pérez and J. M. Soler, Phys. Rev. Lett. **103**, 096102 (2009).

[28]J. Klimeš, D. R. Bowler, and A. Michaelides, J. Phys. Condens. Matter **22**, 022201 (2010).

[29]J. S. Shah and M. E. Straumanis, J. Appl. Phys. **42**, 3288 (1971).

[30]G. Henkelman, B. P. Uberuaga, and H. Jónsson, J. Chem. Phys. **113**, 9901 (2000).

[31]G. Henkelman and H. Jónsson, J. Chem. Phys. **113**, 9978 (2000).

[32]A. De Vita, I. Štich, M. J. Gillan, M. C. Payne, and L. J. Clarke, Phys. Rev. Lett. **71**, 1276 (1993).

[33]I. Štich, M. C. Payne, A. De Vita, M. J. Gillan, and L. J. Clarke, Chem. Phys. Lett. **212**, 617 (1993).

[34]I. Štich, A. De Vita, M. C. Payne, M. J. Gillan, and L. J. Clarke, Phys. Rev. B **49**, 8076 (1994).

[35]A. Groß and A. Dianat, Phys. Rev. Lett. **98**, 206107 (2007).

[36]L. S. Dubrovinsky and S. K. Saxena, Phys. Chem. Miner. **24**, 547 (1997).

[37]X. Qian and W. Hübner, Phys. Rev. B **60**, 16192 (1999).

[38]H. L. Meyerheim, D. Sander, R. Popescu, P. Steadman, S. Ferrer, and J. Kirschner, Surf. Sci. **475**, 103 (2001).

[39]W. L. Hayes, *Statistics* (Holt, Rinehart and Winston, 1981).

[40]Q. J. Zhang, J. C. Lin, N. Shamir, and R. Gomer, Surf. Sci. **231**, 344 (1990).

[41]B. Baule, Annalen der Physik **349**, 145 (1914).